Natural Resources for Human Health
eISSN: 2583-1194

Original Research

Received 23 July 2026
Revised 19 Aug 2026
Accepted 06 Sep 2026

Natural Resources for Human Health 2026, Vol. 6 (20s): 1484–1500

KEYWORDS:
Groundwater; Hydrochemistry; Mineralization; Nitrates; Water Quality

Physico-Chemical Assessment of Groundwater from wells and Boreholes in three Agricultural Regions of the Sétif High Plains, North-Eastern Algeria

Benzidane Chahrazed [1]*, Rouabhi Amar2, Zouaoui Rabea3, Fenni Mouhamed4, Bouharati Sedek4 et Rahmouni Malika4

[1] Faculty of Natural and Life Sciences. Department of Basic study UFAS, Sétif 1 University, Algeria
[2]Faculty of Natural and Life Sciences. Department of Agronomie UFAS, Sétif 1 University, Algeria
[3]Laboratory of Valorization and Bioengineering of Natural Resources (LVBRN), Faculty of Sciences, University of Algiers, Algiers, Algeria
[4]Faculty of Natural and Life Sciences. Department of ecology UFAS, Sétif 1 University, Algeria

ABSTRACT: In the Hautes Plaines region of Sétif (northeastern Algeria), preserving groundwater quality is a major challenge for the drinking water supply. This study aims to assess the physicochemical quality and analyze the spatiotemporal dynamics of water from wells and boreholes in three agricultural municipalities: Mezloug (S1), Guellal (S2), and Bir Haddada (S3). A total of 90 samples were collected during two seasonal campaigns—one in winter and one in summer—between 2017 and 2018. Sixteen physicochemical parameters were analyzed using the Rodier method and compared to JORA and WHO standards. Descriptive statistics and principal component analysis (PCA) were performed. The results revealed high mineralization, with electrical conductivity (EC) values ranging from 4.33 to 8,460 µS/cm and TDS concentrations ranging from 518 to 5,500 mg/L. Stations S1 and S2 exhibited high hardness, with maximum values of 4,800 mg/L at station S1, as well as high concentrations of calcium (569.20 mg/L), chlorides (1481.93 mg/L), and sulfates (485 mg/L at station S1). Nitrate contamination was of particular concern at station S1, with a maximum of 88.55 mg/L of NO_3^-, exceeding the limit of 50 mg/L, while nitrite concentrations sometimes reached 0.60 mg/L. These variations result from the interaction between natural hydrogeochemical processes and diffuse anthropogenic inputs associated with agricultural activities, hence the need for monitoring and more rational management of natural resources

1. INTRODUCTION

Access to safe drinking water is a basic human need and a fundamental right for all people on Earth (Abascal et al., 2022; Derdour et al., 2023). Freshwater accounts for only 2.5% of all the water on Earth, and nearly 30.1% of this small amount is stored as groundwater (Abascal et al., 2022). Globally, approximately 50% of drinking water and nearly 40% of irrigation water come from these underground aquifers (Abascal et al., 2022); in semi-arid regions, these groundwater resources play a crucial role in meeting domestic, agricultural, and industrial needs (Nadjai et al., 2024), often constituting the only available source of water to alleviate chronic shortages (Nadjai et al., 2024; Derdour et al., 2023).

Natural Resources for Human Health
eISSN: 2583-1194

Preserving the quality of groundwater resources, as the use of degraded water poses serious health risks to humans (Nadjai et al., 2024); the qualitative assessment of the resource is based on the analysis of its physical, chemical, and biological characteristics (Derdour et al., 2023); the fundamental physical properties are characterized by temperature, pH, electrical conductivity (EC), and total dissolved solids (TDS) content (Nadjai et al., 2024). Chemically, the resource is defined by the concentrations of its major cations (Ca^{2+}, Mg^{2+}, Na^{+}, K^{+}) and major anions (Cl^{-}, SO_4^{2-}, HCO_3^{-}, NO_3^{-}) (Nadjai et al., 2024).

The natural hydrochemical composition of groundwater is intrinsically determined by the geology and mineralogical composition of aquifers, as well as by the interactions between water and rock and by the residence time of the water in the subsurface (Abascal et al., 2022; Derdour et al., 2023). These phenomena govern the dissolution and sequential precipitation of key minerals such as calcite, dolomite, halite, gypsum, and anhydrite (Selmane et al., 2023; Derdour et al., 2023). Furthermore, under arid climatic conditions, intense evaporation acts as a predominant hydrological factor, causing a natural increase in water mineralization—an effect that is all the more pronounced when the water table is shallow (Nadjai et al., 2024; Medjani et al., 2021). In addition to these natural factors, human activities are exerting increasing pressures that degrade groundwater quality (Abascal et al., 2022); these anthropogenic pressures manifest themselves notably through intensive agriculture, via the widespread use of chemical fertilizers and pesticides to increase crop yields (Rawat et al., 2022). Other sources of degradation include leaks from septic tanks, leaching from municipal solid waste landfills, and the infiltration of untreated domestic or industrial wastewater (Abascal et al., 2022; Nadjai et al., 2024; Mora et al., 2022); nitrate (NO_3^{-}) is the most ubiquitous and mobile anthropogenic pollutant in aquifers; its ingestion through drinking water poses a serious health threat, as it can cause methemoglobinemia in newborns (Abascal et al., 2022; Mora et al., 2022).

In Algeria, In Algeria, human and agro-economic dependence on groundwater resources is extremely high (Derdour et al., 2023); unfortunately, Algerian aquifers are facing severe spatiotemporal degradation due to overexploitation and diffuse pollution (Nadjai et al., 2024); (Selmane et al., 2023), assessments conducted across the country—whether in the Moyen-Chellif Plain (Nadjai et al., 2024), the Maadher Plain in Hodna (Selmane et al., 2023), the Ain Sefra basin (Derdour et al., 2023), the Mougheul region (Mebarki et al., 2021), or the shallow aquifers of Ouargla (Medjani et al., 2021), all indicate recurring exceedances of water quality standards. These studies report critical concentrations of nitrates, sulfates, calcium, and chlorides that regularly exceed the regulatory limits set by the WHO for drinking water (Selmane et al., 2023; Nadjai et al., 2024); (Mebarki et al., 2021) or the shallow aquifers of Ouargla (Medjani et al., 2021) all indicate recurring exceedances of water quality standards. (Mebarki et al., 2021). In northeastern Algeria, the Setif region is characterized by intense agricultural activity, where the water supply depends heavily on groundwater, as evidenced by the plains in the eastern part of the region, such as the Bazer Sakhra area (Bounab et al., 2022), this local context raises serious hydrochemical issues, as the intensive use of water from wells and boreholes compromises its suitability for human consumption and irrigation due to the increasing infiltration of agricultural and urban effluents (Bounab et al., 2022).

Despite the urgency of this situation, there remains a major scientific gap regarding the implementation of continuous, integrated spatiotemporal hydrochemical monitoring in Algeria's semi-arid climate (Derdour et al., 2023; Rawat et al., 2022). Existing hydrogeological studies often remain fragmented and lack consistency, particularly with regard to the rigorous monitoring of seasonal variations in total mineralization and the transport of agricultural pollutants (Derdour et al., 2023; Rawat et al., 2022); the absence of a unified local database and precise conceptual models hinders policymakers' ability to develop sustainable resource protection plans (Nadjai et al., 2024); (Derdour et al., 2023; Rawat et al., 2022).

To address this gap, the main objective of this study is to assess the physicochemical quality of well and borehole water in the Sétif region; more specifically, it aims to characterize the spatial variations and seasonal fluctuations (winter and summer) of physical parameters and key chemical components (T, pH, conductivity, TDS, turbidity, dissolved oxygen, total hardness, major cations and anions, and nitrogen compounds). The collected data will be compared with WHO recommendations and Algerian JORA standards to determine the suitability of these waters for human consumption, thereby providing a decision-support framework for the sustainable management of regional water resources.

2. MATERIALS AND METHODS

2.1 Study area and sampling strategy

The geographical setting of the Setif region served as the basis for this study. Located in the high plains of eastern Algeria, it is a region with significant agricultural activity, particularly in the areas of cereal farming and livestock raising. Sétif is located in a

semi-arid bioclimatic zone with a predominantly continental climate, characterized by hot, dry summers. The locations selected for our study stretch along the territory from Mezloug to Sersoub Bir Hadada, where water quality was tested in wells and boreholes: Mezloug (station S1), Guellal (station S2), and Bir Haddada (station S3).

A total of 90 water samples were collected from the three stations during the 2017–2018 period. The sampling strategy consisted of two seasonal campaigns: a winter/rainy season campaign (September through December) and a summer/dry season campaign (April through August).

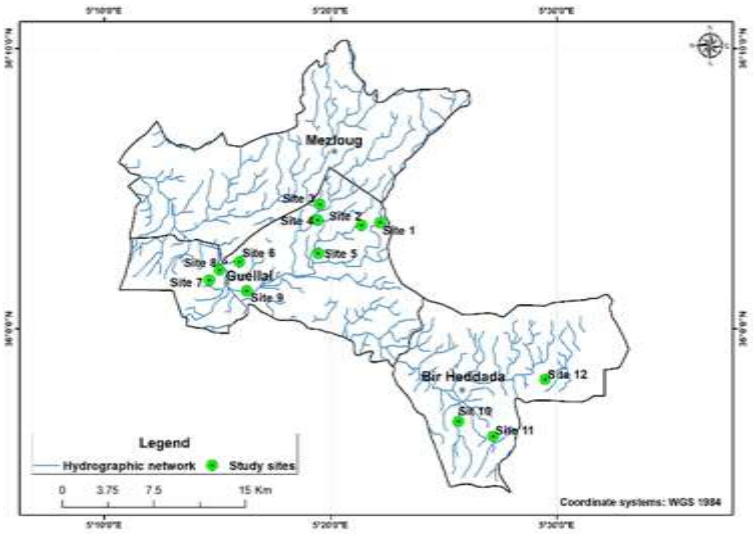


Figure 1. Location of the study sites and hydrographic in the Mezloug, Guellal and Bir Haddada regions, northeastern Algeria

2.2 Sample Collection and preparation

Water samples were collected at least 30 cm below the water's surface to avoid surface contamination. The samples were collected in 1-liter polyethylene bottles that had been cleaned and rinsed beforehand. Immediately after collection, the bottles were sealed tightly, placed in an insulated cooler at 4 °C, and then transported to the laboratory, where they were filtered through a nitrocellulose membrane with a pore size of 0.45 µm, in accordance with standard procedures.

2.3 Physico-chemical analyses

The assessment of water quality is based on the analysis of 18 physicochemical and organoleptic parameters, measured in accordance with the methods of Rodier (2009) and compared to the standards of the World Health Organization (WHO, 2014) and Algerian regulations (JORA, 2014).

2.4 Analytical Methods

Temperature (°C) and hydrogen ion concentration (pH) were measured using a HANNA 211 pH meter/thermometer. Electrical conductivity (EC, expressed in µS/cm at 20 °C) was measured in situ using an LF 538WTW conductivity meter. Turbidity (expressed in NTU) was determined in the laboratory using a HANNA 14 turbidimeter. Color was assessed by visual inspection, odor by smell, and taste by tasting at the time of sampling. Dissolved oxygen (DO, mg/L), total dissolved solids (TDS, mg/L), salinity (SAL, %), and redox potential (ORP, mV) were determined using a probe/ multiparameter kit (Aqua Read AP 2000 version 1.04–4.54, Doc No. 10401 00870, AQUAREAD Ltd.). Calcium (Ca^{2+}) and total hardness (TH): determined by complexometric titration with EDTA in the presence of specific color indicators. Magnesium (Mg^{2+}): calculated as the difference between total hardness (TH) and the calcium (Ca^{2+}) concentration.

Chlorides (Cl^-): Determined by titration using the Mohr method with a silver nitrate ($AgNO_3$) standard solution in a neutral medium, in the presence of potassium chromate. Bicarbonates (HCO_3^-): Determined by titration with sulfuric acid (total alkalinity, TAC). Nitrates (NO_3^-), nitrites (NO_2^-), sulfates (SO_4^{2-}), orthophosphates (PO_4^{3-}), : Determined using the methods recommended by Rodier (2009).

Natural Resources for Human Health
eISSN: 2583-1194

2.5 Statistical Analysis

The collected data were subjected to descriptive statistical analysis (means, standard deviations, minimum and maximum values) using XLSTAT software. To summarize the spatio-temporal variability and identify the main factors influencing mineralization and water pollution, a principal component analysis (PCA) was performed using SPSS software (version 26.0) based on the physicochemical data matrices.

3. RESULTS AND DISCUSSION

3.1 Physical properties and oxidation state

Spatio-temporal variation in temperature (T °C)

The results show that these temperatures generally range from 10.1 °C to 25.50 °C, the calculated average values are 18.69 °C (±0.76) at station S1, 18.72 °C (±0.72) at station S2, and 19.27 °C (±0.79) at station S3.

Spatio-temporal variation in hydrogen ion concentration (pH)

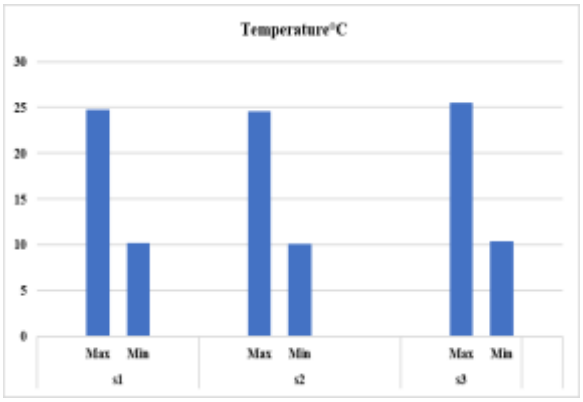
pH measurements range from 6.50 to 9.32, indicating water that is neutral to distinctly alkaline. Station S1 recorded the highest average value at 8.82 (±0.13) (min 6.55; max 9.32), followed by station S2 at 8.02 (±0.10) (min 6.98; max 8.99) and station S3 at 7.66 (±0.12) (min 6.50; max 8.99).

Spatio-temporal variation in turbidity

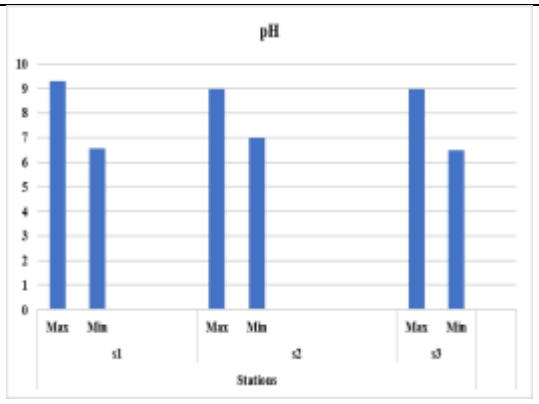
Average turbidity remains low at stations S1 (0.78 NTU) and S2 (0.63 NTU), but reaches 2.72 NTU at station S3. Whilst the vast majority of samples remain below the maximum permissible limit of 5 NTU set by WHO, pronounced seasonal peaks were recorded during the winter period, rising to 6.90 NTU at station S2 and as high as 33.40 NTU at station S3.

Spatio-temporal variation in dissolved oxygen (DO)

Dissolved oxygen concentrations generally fluctuate between 2.28 mg/L and 12.03 mg/L. Station S1 has an average of 8.76 mg/L (±0.22) (7.32 to 12.03 mg/L), station S2 records 8.47 mg/L (±0.19) (6.94 to 11.36 mg/L) and station S3 recorded 7.12 mg/L (±0.31) (2.28 to 11.05 mg/L).

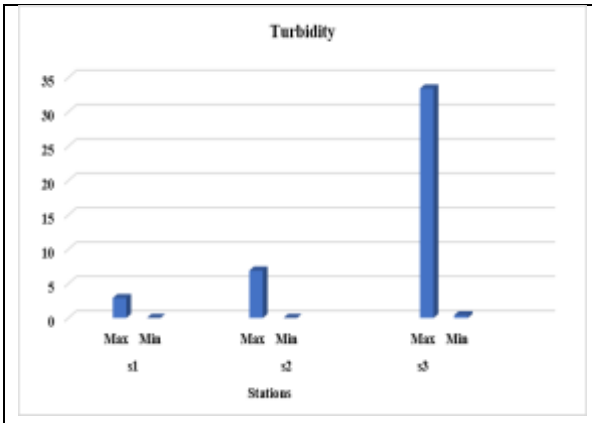


A. Spatiotemporal variation in temperature (°C) across the different sites

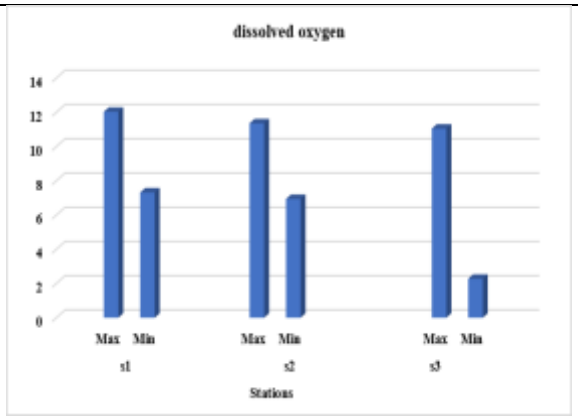


B. Spatiotemporal variation in water pH across the different sites

Natural Resources for Human Health
eISSN: 2583-1194



C. Spatiotemporal variation in turbidity



D. Spatiotemporal variation in dissolved oxygen

Figure 2. Physical parameters and oxidation state

3.2 Total mineralisation and salt content

Spatio-temporal variation in electrical conductivity (EC)

Electrical conductivity shows a very wide range of variation, ranging from 4.33 to 8,460.00 µS/cm. The average value is 1,334.29 µS/cm (±145.05) at station S1 (81.50 to 3,716.00 µS/cm), 2,251.54 µS/cm (±285.51) at station S2 (4.33 to 8,460.00 µS/cm) and 1,920.77 µS/cm (±158.01) at station S3 (399.00 to 4,021.00 µS/cm).

Spatio-temporal variation in total dissolved solids (TDS)

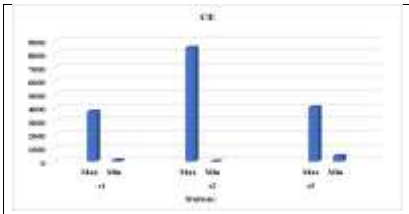
The total dissolved solids content ranges from 518.00 mg/L to 5,500.00 mg/L, with average concentrations of 1,271.93 mg/L (±88.98) for S1 (718.00 to 2,613.00 mg/L), 1,293.00 mg/L (±162.79) for S2 (707.00 to 5,500.00 mg/L) and 805.57 mg/L (±41.18) for S3 (518.00 to 1,422.00 mg/L).

Spatio-temporal variation in total hardness (TH)

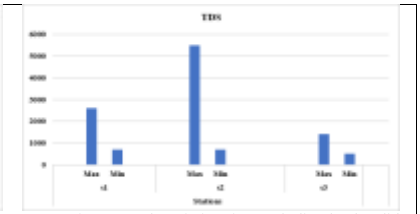
The total hardness values show marked spatial variation: station S1 recorded an average of 1,195.30 mg/L (±165.02) (340.00 to 4,800.00 mg/L), station S2 an average of 437.27 mg/L (±40.40) (260.00 to 1,295.00 mg/L), and station S3 an average of 200.47 mg/L (±20.97) (42.10 to 505.00 mg/L).

Spatio-temporal variation in salinity (SAL)

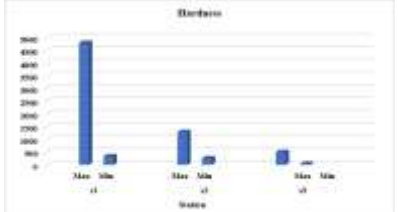
The overall salinity ranges from 0.22 g/L to 4.69 g/L. The average is 0.91 g/L (±0.14) at S1 (max 4.69 g/L), 0.69 g/L (±0.04) at S2 (0.22 to 1.11 g/L) and 1.07 g/L (±0.09) at S3 (0.52 to 2.20 g/L).



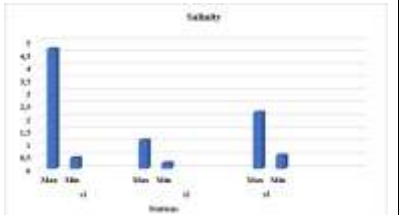
5. Spatiotemporal variation in electrical conductivity (µS/cm)



B. Spatiotemporal variation in total dissolved solids (TDS)



C. Spatiotemporal variation in total hardness (TH)



D. Spatiotemporal variation in salinity

Figure 3. Overall mineralization and salinity load

Natural Resources for Human Health
eISSN: 2583-1194

3.3 Ionic facies, major cations and anions

Spatio-temporal variation in calcium (Ca^{2+})

Calcium concentrations range from 48.90 mg/L to 569.20 mg/L, with station averages of 202.12 mg/L at S1 (86.20 to 569.20 mg/L), 192.50 mg/L at S2 (48.90 to 428.85 mg/L) and 156.41 mg/L at S3 (72.57 to 272.10 mg/L).

Spatio-temporal variation in magnesium (Mg^{2+})

Magnesium concentrations range from 41.50 mg/L to 273.22 mg/L. The average is 132.09 mg/L at S1 (70.38 to 267.30 mg/L), 132.29 mg/L at S2 (53.46 to 273.22 mg/L) and 100.39 mg/L at S3 (41.50 to 171.00 mg/L).

Spatio-temporal variation in chlorides (Cl^-)

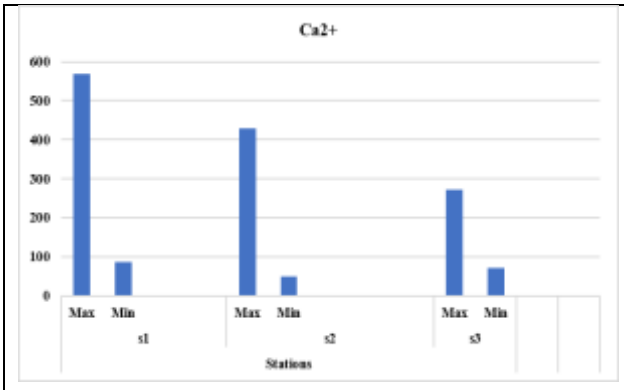
Chloride concentrations show very marked variations, ranging from 28.40 mg/L to 1,481.93 mg/L. Monitoring station S1 recorded the highest average value (489.76 mg/L) with a peak of 1,481.93 mg/L, indicating a marked deterioration beyond the JORA regulatory threshold (500 mg/L). Stations S2 (42.60 to 519.30 mg/L) and S3 (28.40 to 493.50 mg/L) remain broadly compliant.

Spatio-temporal variation in bicarbonates (HCO_3^-)

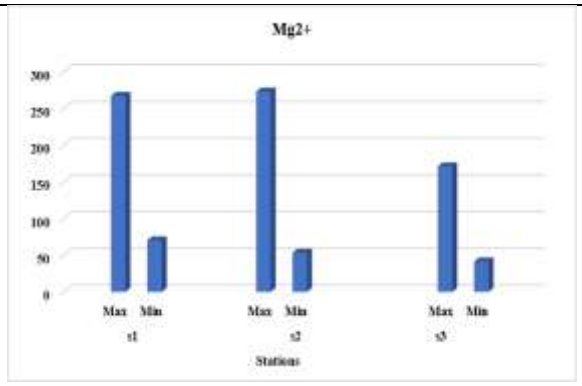
Bicarbonate concentrations range from 4.00 mg/L to 744.00 mg/L (expressed as $CaCO_3$). The ranges recorded are 8.00–744.00 mg/L at S1, 5.10–537.00 mg/L at S2 and 4.00–346.00 mg/L at S3, with higher peaks in winter.

Spatio-temporal variation in sulfate ion (SO_4^{2-})

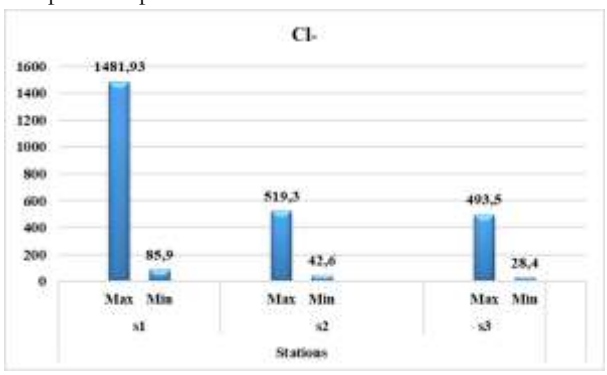
The sulfate ion (SO_4^{2-}) concentrations recorded in the first series show high values ranging from 71.82 mg/L to 485.00 mg/L, with an average of 296.18 mg/L. The second series had an average concentration of 146.00 mg/L (with extreme values of 39.60 mg/L and 359.00 mg/L), while the third series show more moderate levels, characterized by an average of 64.73 mg/L (ranging from 12.50 mg/L to 234.60 mg/L).



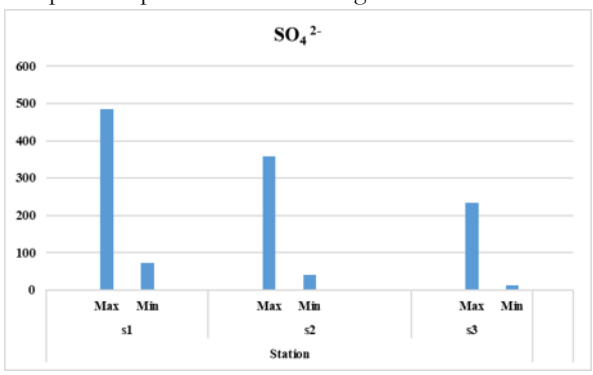
A. Spatiotemporal variation in calcium concentration



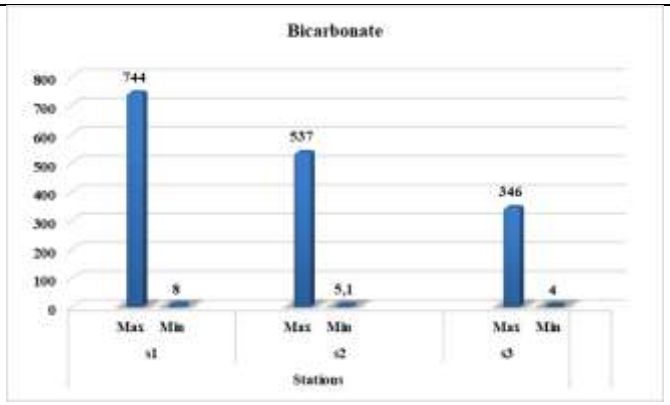
B. Spatiotemporal variation in magnesium concentration



C. Spatiotemporal variation in chloride concentration



D. Spatiotemporal variation in sulfate concentration



E. Spatiotemporal variation in bicarbonate concentration

Figure 4. Ionic facies, major cations and anions

3.4. Nutrients and human-induced pollution

Spatio-temporal variation in nitrates (NO_3^-)

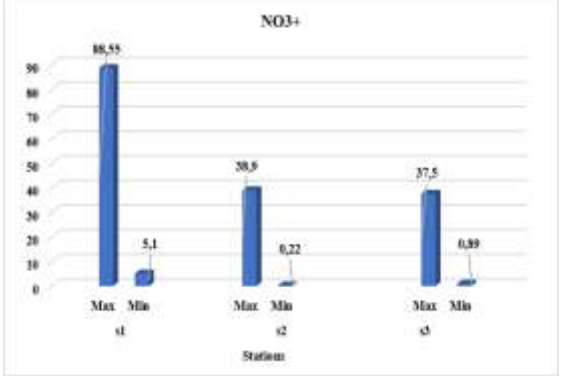
Nitrate concentrations range from 0.22 mg/L to 88.55 mg/L. Monitoring point S1 is clearly affected by nitrate pollution, with a maximum concentration of 88.55 mg/L, exceeding the drinking water standard of 50 mg/L set by the WHO and JORA. By contrast, stations S2 (0.22 to 38.90 mg/L) and S3 (0.89 to 37.50 mg/L) remain fully compliant.

Spatio-temporal variation in nitrites (NO_2^-)

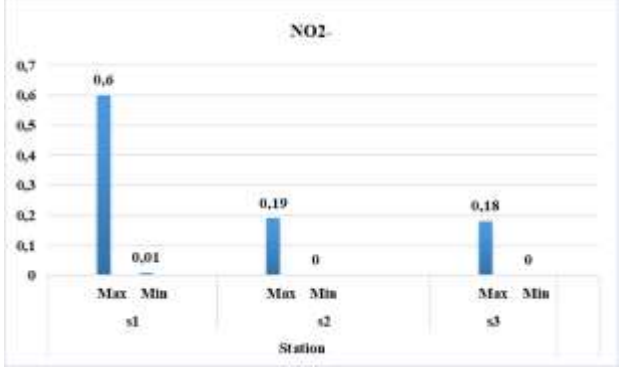
Nitrite concentrations remain very low overall, ranging from 0.00 mg/L to 0.60 mg/L. Monitoring points S2 (0.00 to 0.19 mg/L) and S3 (0.00 to 0.18 mg/L) are fully compliant with the regulatory limit of 0.2 mg/L. Station S1 is the only one to show occasional exceedances reaching 0.60 mg/L.

Spatio-temporal variation in orthophosphates (PO_4^{3-})

Orthophosphate concentrations are moderate and consistently below the environmental quality threshold of 5 mg/L. They range from 0.10 to 1.80 mg/L at S1, from 0.03 to 1.82 mg/L at S2 (absolute maximum) and from 0.01 to 0.60 mg/L at S3.

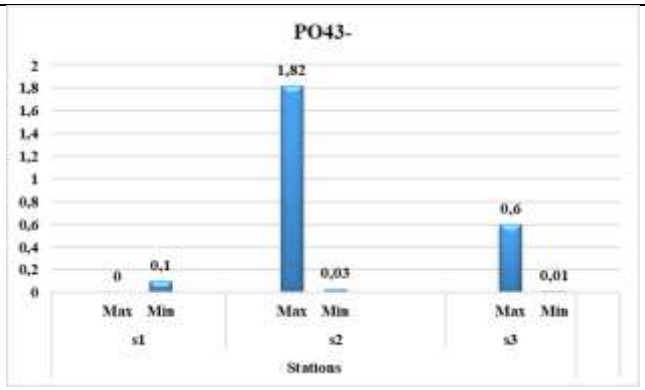


A. Spatiotemporal variation in nitrate concentration



B. Spatiotemporal variation in nitrite concentration

Natural Resources for Human Health
eISSN: 2583-1194



C. Spatiotemporal variation in orthophosphate (PO_4^{3-}) concentration

Figure 5. Nutrients and anthropogenic pollution

3.5. Seasonal and spatial dynamics from upstream to downstream

Seasonal comparison of Ca^{2+}, Mg^{2+} and NO_3^- ions (WIN versus SUM)

Concentrations of calcium (Ca^{2+}) and magnesium (Mg^{2+}) remained at high levels throughout both seasons, confirming a stable chemical profile. In contrast, nitrate (NO_3^-) reached its highest peaks during the winter campaign (WIN) at station S1 (> 50 mg/L).

Seasonal comparison of turbidity and salinity (WIN versus SUM)

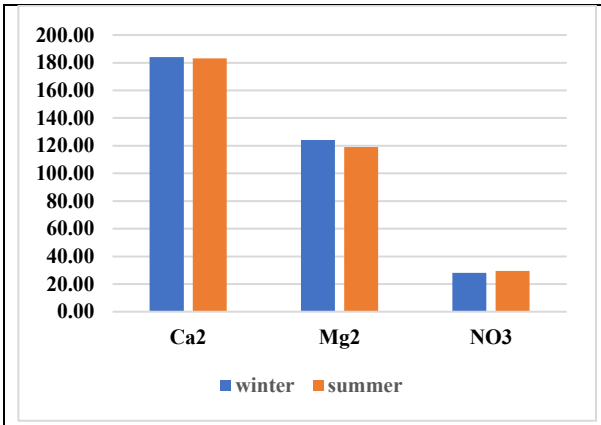
Turbidity tends to rise during the winter period (WIN), particularly at stations S3 (33.40 NTU) and S2 (6.90 NTU). This phenomenon is caused by particulate matter carried by surface runoff and the rapid infiltration of rainfall. Salinity follows the dynamics of solutes (0.22 to 4.69 g/L),

Upstream-downstream spatio-temporal dynamics (WIN, SUM, SE-WIN, SE-SUM)

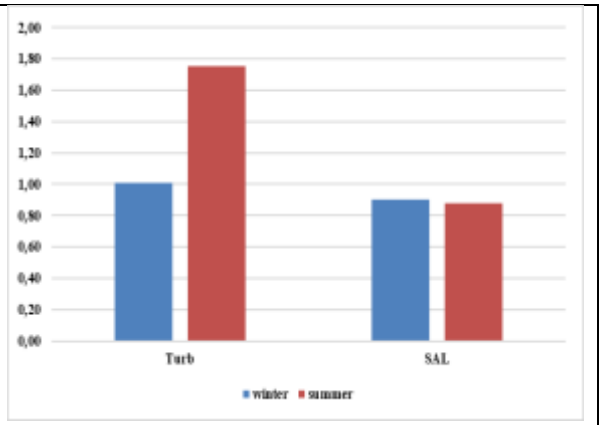
The overall spatio-temporal analysis highlights a gradual change in mineralisation along the flow lines, from upstream to downstream (SE), in line with the seasonal cycle (WIN/SUM). Downstream (SE-WIN and SE-SUM), the majority of dissolved solutes and electrical conductivity are higher than at upstream sites. Furthermore, winter sampling campaigns (WIN and SE-WIN) frequently show higher concentrations of major ions (Cl^-, SO_4^{2-}, HCO_3^-) than in summer.

Seasonal comparison of total mineralisation, TDS, EC, TH and Cl^- (WIN versus SUM)

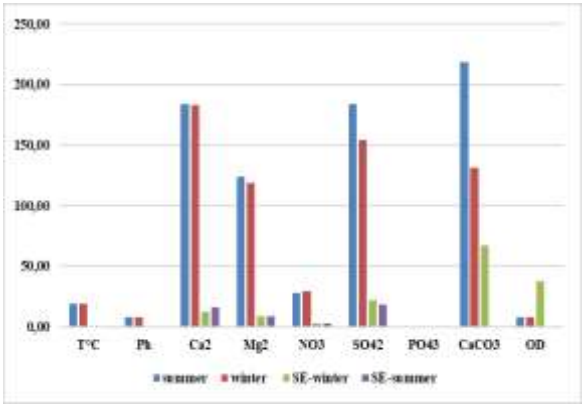
A comparison of the mineralisation parameters (TDS, CE, TH and Cl^-) confirms that values were higher during the winter campaign (WIN) than during the summer campaign (SUM).



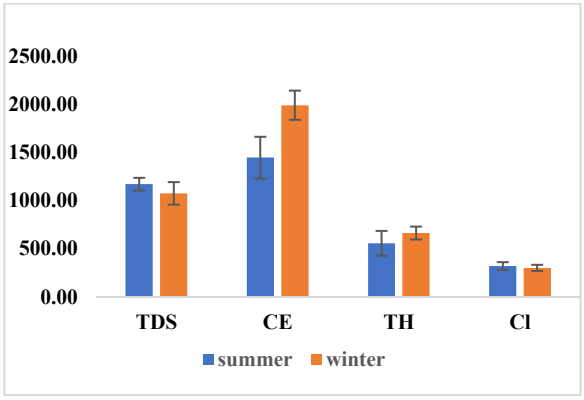
A. Comparison of ion concentrations (Ca^{2+}, Mg^{2+}, NO_3^-) between winter (WIN) and summer (SUM)



B. Comparison of turbidity and salinity between winter (WIN) and summer (SUM)



C. Comparison of the physicochemical parameters of water samples from WIN, SUM, SE-WIN, and SE-SUM



D. Comparison of total dissolved solids (TDS), electrical conductivity (EC), total hardness (TH), and chloride (Cl^-) concentrations between summer (SUM) and winter (WIN)

Figure 6. Seasonal (WIN and SUM) and spatial (downstream) dynamics

3.6. Correlation Analysis of Groundwater Parameters

A Pearson correlation matrix was computed to evaluate the linear relationships among the various physicochemical parameters of groundwater. The key associations between these variables are highlighted in the table1. below.

Table 1. Pearson Correlation Matrix Among the Physicochemical Parameters of Groundwater.

	T°C	pH	TDS	CE	Turb.	TH	SAL	Ca2+	Mg2+	NO3+	NO2-	SO42-	PO43-	Cl-	CaCO3	OD
T°C	1	-,352**	-0,017	-0,058	-,259*	-0,090	0,029	-,856**	-,825**	-0,122	-,221*	-,473**	-,477**	-,581**	-,254*	-,572**
pH			0,154	-0,158	-0,099	,499**	-0,019	,402**	,342**	,323**	,352**	,663**	,432**	,513**	0,205	,462**
TDS			1	-0,080	-0,056	0,052	-0,041	0,037	-0,039	0,174	0,141	,227*	0,048	0,081	0,034	0,148
CE				1	-0,070	-0,178	-0,027	-0,030	-0,066	-,238*	-0,113	-0,199	-0,075	-0,100	0,031	-0,090
Turb.					1	-0,100	-0,026	0,118	0,066	-0,010	-0,099	-0,043	-0,107	0,084	,301*	0,172
TH						1	-0,137	0,143	0,164	,331**	,278**	,531**	,318**	,315**	0,137	,256*

SAL							1	-0,049	-0,098	-0,023	,229*	0,057	-0,052	0,065	0,017	-0,163
Ca2+								1	,932**	0,110	,260*	,554**	,610**	,655**	,334**	,631**
Mg2+									1	0,110	,236*	,564**	,635**	,584**	,319*	,624**
NO3+										1	,460**	,464**	0,211	,270*	0,086	0,158
NO2-											1	,482**	,296**	,257*	,248*	0,205
SO42-												1	,577**	,646**	,297*	,580**
PO43-													1	,514**	,271*	,635**
Cl-														1	,280*	,562**
CaCO3															1	,293*
OD																1

The values shown correspond to Pearson's correlation coefficients (r). * Significant correlation at $p < 0.05$; ** significant correlation at $p < 0.01$.

The correlation matrix reveals several significant relationships between the physico-chemical parameters of groundwater. The strongest correlation is observed between Ca^{2+} and Mg^{2+} (r = 0.932), indicating that the concentrations of these two ions are closely linked. Positive correlations are also observed between Ca^{2+} and SO_4^{2-} (r = 0.554), PO_4^{3-} (r = 0.655) and $CaCO_3$ (r = 0.631), as well as between Mg^{2+} and PO_4^{3-} (r = 0.635).

Temperature shows several negative correlations, notably with Ca^{2+} (r = -0.856), Mg^{2+} (r = -0.825) and Cl^- (r = -0.581). Furthermore, the nutrients show positive relationships amongst themselves, notably between NO_3^- and NO_2^- (r = 0.460) and between SO_4^{2-} and PO_4^{3-} (r = 0.577). Overall, these correlations highlight significant relationships between the major ions and certain chemical parameters, which may reflect common processes of mineralisation and the geochemical evolution of groundwater.

3.7. Discussion

This temporal distribution reflects the direct influence of ambient microclimatic conditions on a shallow unconfined aquifer. From a regulatory standpoint, all stations comply with the guideline value of 25 °C recommended by the WHO and JORA for human consumption, with the exception of a very minor deviation of 0.5 °C observed in the summer at station S3. These results are consistent with observations made by Aouiti et al. (2021) in Tunisia (10.3 to 24.8 °C), Benmoussa et al. (2020) in the Saoura region (maximum temperatures of 26.5 °C), Mebarki et al. (2021) in Mougheul (24 to 25 °C), and by Selmane et al. (2022a, 2023b) in the Maadher Plain (14.80 to 15.80 °C). However, there is a clear discrepancy with the temperatures recorded by Hakimi et al. (2021) in the Continental Intercalary (25 to 56 °C), by Rahmani & Chibane (2022) in Hammam Charef (40 °C), and by Hamma et al. (2024) at Aïn Ouarka (46 °C); this discrepancy can be explained by the very deep and confined nature of the reservoirs, as well as by water circulation driven by geothermal or hydrothermal gradients.

A high degree of seasonal stability is maintained between the winter and summer sampling campaigns. This alkaline trend stems directly from the dissolution of the carbonate and dolomite rocks comprising the aquifer matrix in a semi-arid climate. The data closely align with the ranges observed by Abdelbaki et al. (2022) at Igli (7.02 to 8.83), Mansouri et al. (2022) at Ouargla (average of 8.00), Ismail et al. (2023) in Egypt (7.74 to 8.60), as well as by other authors in the region (6.7 to 8.5). Conversely, the more acidic pH values reported by Wang et al. (2024) in the Sha River basin (average of 6.71) reflect processes of organic matter oxidation and recharge by non-alkaline surface water.

The baseline values demonstrate the role of physical purification and mechanical filtration provided by the porous soil-reservoir matrix. The winter exceedances observed at shallow wells can be explained by direct surface runoff, rapid rainwater infiltration and the resuspension of sediments during floods or pumping operations. These fluctuations differ from the data reported by Rahmani & Chibane (2022) and Mebarki et al. (2021), where deep sandstone catchments exhibit negligible and constant turbidity.

The measured concentrations are consistently higher during the winter than in the summer. This pattern is governed by the thermodynamic law of inversion between temperature and gas solubility, coupled with increased biological consumption during warmer periods. This behaviour is directly consistent with the work of Medjani et al. (2021) in Ouargla (up to 7.7 mg/L in winter compared with 0.5–4.5 mg/L in summer). In contrast, the local reducing conditions and the stagnation observed at times at station S3 (minimum of 2.28 mg/L) stand in contrast to the constantly re-aerated environments observed in certain fast-flowing alluvial basins.

Many samples exceed the JORA eligibility threshold (2,800 µS/cm) and the WHO guideline value (1,500 µS/cm). This high ionic charge results from the leaching of saline soils, the dissolution of halite and gypsum, and the concentration caused by the re-infiltration of agricultural drainage water. These high values are consistent with those reported by Nadjai et al. (2024) (average of 4,231 µS/cm), Abdelbaki et al. (2022) (up to 14,990 µS/cm) and Bencheikh et al. (2025) (7,180 µS/cm). They contrast with the low conductivities recorded in rapidly recharged sandstone aquifers by Mebarki et al. (2021) (522–1,198 µS/cm) and Hakimi et al. (2021) (340–960 µS/cm).

Stations S1 and S2 far exceed the threshold recommended by the WHO (600 to 1,000 mg/L); this excessive mineralisation is indicative of extensive water rock interactions in the evaporites, combined with surface evaporation. These results fall within the ranges reported by Abdelbaki et al. (2022) (average of 4,652.68 mg/L) and Nadjai et al. (2024) (average of ~2,500 mg/L), but contrast with the fresh waters observed by Mebarki et al. (2021) (402 to 885 mg/L) and Wang et al. (2024) (average of 505 mg/L).

The water at stations S1 and S2 falls into the very hard to excessively hard category, whilst station S3 has moderately hard to hard water. These concentrations are explained by the intense dissolution of limestone, dolomite and gypsum formations. Comparable values are reported by Selmane et al. (2023) (average of 1,203.64 mg/L) and Abdelbaki et al. (2022) (up to 3,960 mg/L), whilst Derdour et al. (2023) observed more moderate values (55.72 mg/L) in a predominantly sandstone environment.

This salt load highlights the vulnerability of shallow structures to evapotranspiration and fertiliser leaching. These levels are consistent with the observations of Aouiti et al. (2021) (0.7 to 6.5 g/L), Ismail et al. (2023) (0.78 to 6.18 g/L) and Bioud et al. (2023), whilst deep confined reservoirs such as the Continental Intercalary (Hakimi et al., 2021) maintain very low salinity levels.

The frequent exceedances of the threshold recommended by the JORA and the WHO (200 mg/L) at stations S1 and S2 reflect the extensive dissolution of limestone, dolomite and gypsum rocks. These results are consistent with the data from Selmane et al. (2022a, 2023b) (108.22 to 601.20 mg/L), Abdelbaki et al. (2022) (46 to 820 mg/L) and Benmoussa et al. (2020) (up to 667 mg/L). They differ from the lower concentrations recorded by Mebarki et al. (2021) (42 to 77 mg/L) and Hakimi et al. (2021) (average of 28 mg/L).

Several samples from stations S1 and S2 exceed the recommended range (100 to 150 mg/L). This enrichment results from the weathering of dolomitic formations and cation exchange mechanisms on clay matrices. These values are consistent with those reported by Nadjai et al. (2024) (up to 306 mg/L) and Selmane et al. (2022a, 2023b) (36.46 to 255.20 mg/L), but significantly exceed the concentrations reported by Derdour et al. (2023) (average of 56.21 mg/L) and Mohammed et al. (2022) (14.6 to 54 mg/L).

The excess of chlorides at S1 stems from the dissolution of halite (NaCl), the leaching of saline soils under high evaporation rates, and anthropogenic discharges. These observations are consistent with those of Nadjai et al. (2024) (111 to 2,400 mg/L), Abdelbaki et al. (2022) (40 to 2,500 mg/L) and Hamma et al. (2024) (110 to 2,710 mg/L), contrasting sharply with the very low-salinity waters of Mougheul (Mebarki et al., 2021: 13 to 30 mg/L). F. Spatio-temporal variation in sulphates (SO_4^{2-}) Sulphate concentrations rise to 485.00 mg/L at station S1, with averages of 296.18 mg/L (S1), 359.00 mg/L (S2) and 234.60 mg/L (S3). Station S1 approaches or exceeds the WHO (250 mg/L) and JORA (400 mg/L) guideline thresholds. These high concentrations can be explained by the dissolution of gypsum lenses and anhydrite contained within the rock formation, combined with the return of irrigation water. These trends are corroborated by Nadjai et al. (2024) (up to 1,670 mg/L) and Abdelbaki et al. (2022) (40 to 3,500 mg/L), whilst Rahmani & Chibane (2022) (average of 163.06 mg/L) and Hakimi et al. (2021) (30 to 200 mg/L) report lower concentrations due to the absence of major gypsum formations.

This enrichment results from the weathering of calcareous-dolomitic formations by carbon dioxide dissolved in the soil. These results are in perfect agreement with the ranges reported by Nadjai et al. (2024) (46 to 860 mg/L), Benmoussa et al. (2020) (70 to 471 mg/L) and Abdelbaki et al. (2022) (37 to 366 mg/L).

The concentrations of sulfate ions (SO_4^{2-}) measured in the analyzed water samples show significant variations from one monitoring station to another or from one sampling campaign to another. This spatial and temporal distribution reflects the heterogeneity of groundwater mineralization, which is likely influenced

The contamination at S1 results from the leaching of synthetic nitrogen fertilisers applied to surrounding crops, combined with leaks from domestic wastewater and on-site sewage systems. Similar exceedances are reported by Selmane et al. (2022a, 2023b) (average of 173.47 mg/L), Nadjai et al. (2024) (>80% exceedance), Bencheikh et al. (2025) and Brella et al. (2023). Conversely, Abdelbaki et al. (2022) (average of 42.11 mg/L), Derdour et al. (2023) (average of 26.51 mg/L) and Hakimi et al. (2021) (< 1 mg/L) report low concentrations, which can be explained by areas with little agricultural activity or effective hydrogeological protection of confined aquifers.

The fact that 98 per cent of samples comply confirms the absence of widespread fresh nitrogen contamination. As the nitrite ion is unstable, it oxidises rapidly to nitrate in aerated unconfined aquifers. The peaks recorded at S1 reflect a direct, very localised gross anthropogenic input (septic tanks or slurry) injected near the well before complete nitrification has taken place. These data validate the findings of Selmane et al. (2022a, 2023b) (0.0008 to 0.02 mg/L) and the reviews by Abascal et al. (2022).

These low concentrations indicate limited phosphate pollution. As highlighted by Abascal et al. (2022) and Wang et al. (2024), surface-applied phosphates exhibit very limited mobility in the unsaturated zone due to their rapid fixation and adsorption onto ferro-aluminium and clay complexes in the soil, limiting their transfer to the groundwater compared with nitrates.

This winter behaviour can be explained by the direct transport of nitrogen fertilisers and surface residues via rainwater percolation. This winter dynamic is consistent with the findings of Nadjai et al. (2024), Selmane et al. (2022a, 2023b) and Abascal et al. (2022).

Fluctuating in line with soil leaching in winter and concentration through evapotranspiration in summer. These variations are consistent with observations made in semi-arid environments by Aouiti et al. (2021), Bioud et al. (2023) and Medjani et al. (2021).

The downstream increase is explained by the prolonged residence time of the water, which favours the continuous dissolution of the rock matrix, coupled with the accumulation of anthropogenic discharges along the catchment. The winter overconcentrations result from intense soil leaching and the flushing of the unsaturated zone by rainfall recharge. These results are in direct agreement with Nadjai et al. (2024), Brella et al. (2023) and Ismail et al. (2023). However, they contrast with the observations of Aouiti et al. (2021) in Tunisia, where rainfall recharge produces a predominant dilution effect.

Winter rainfall percolating through the saline soil cover intensively solubilises evaporite minerals (halite, gypsum) and leaches the salt load accumulated in the soils. These observations are supported by Nadjai et al. (2024) (EC of 4,153 µS/cm during the wet season compared with 4,231 µS/cm during the dry season), Selmane et al. (2022a, 2023b) and Bencheikh et al. (2025), whilst deep sandstone aquifers (Mebarki et al., 2021; Hakimi et al., 2021) remain unaffected by these surface dynamics.

Analysis of the Pearson correlation matrix presented in Table 1 enables the identification of the main geochemical mechanisms, mineral dissolution processes and anthropogenic influences that may govern groundwater quality.

A very strong positive correlation was observed between calcium (Ca^{2+}) and magnesium (Mg^{2+}) ($r = 0.932$, $p < 0.01$), accompanied by positive correlations between Ca^{2+} and $CaCO_3$ ($r = 0.631$) and with total hardness (TH). This interdependence suggests a common geochemical origin linked to the simultaneous weathering and dissolution of carbonate rocks, notably calcite and dolomite. This result is consistent with the work of Brindha et al., who report a highly significant positive correlation between Ca^{2+} and Mg^{2+} ($r = 0.81$). It is also consistent with the study of the Qatar aquifer, where the parallel trends in calcium and magnesium confirm a common hydrogeochemical control associated with mineral weathering processes.

The relationships between the major cations and anions show moderate to strong positive correlations between Ca^{2+} and SO_4^{2-} ($r = 0.554$), Ca^{2+} and Cl^- ($r = 0.655$), as well as between Mg^{2+} and PO_4^{3-} ($r = 0.635$), Mg^{2+} and SO_4^{2-} ($r = 0.564$) and Mg^{2+} and Cl^- ($r = 0.584$). The associations between Ca^{2+}, SO_4^{2-} and Cl^- may reflect the dissolution of evaporite minerals, notably gypsum ($CaSO_4 \cdot 2H_2O$) and halite (NaCl), during water–rock interaction. This result is consistent with the observations by Kada et al. at Ain Azel, where Ca^{2+} shows correlations with SO_4^{2-} ($r = 0.67$) and Cl^- ($r = 0.64$). It is also consistent with the study from Qatar, which reports correlations of $r = 0.71$ between Ca^{2+} and Cl^- and $r = 0.82$ between Ca^{2+} and SO_4^{2-}, confirming the importance of the dissolution of sulphates and chlorides in the release of calcium.

Temperature (T°C) shows very strong negative correlations with Ca^{2+} ($r = -0.856$), Mg^{2+} ($r = -0.825$), Cl^- ($r = -0.581$) and dissolved oxygen (DO) ($r = -0.572$). pH, on the other hand, is positively correlated with SO_4^{2-} ($r = 0.663$), Cl^- ($r = 0.513$) and TH ($r = 0.499$). The relationship between temperature and mineralisation differs from that observed in the Oued Souf aquifer by Barkat et al., where no predominant negative correlation with total mineralisation is reported; this may reflect conditions of direct meteoric recharge and different thermal dynamics in a shallow aquifer. The relationship with pH is partly consistent with the Ain Azel study, which reports a correlation of $r = 0.63$ between pH and bicarbonates, illustrating the neutralisation and alkalisation effects during the dissolution of carbonates. However, it differs from the study conducted in areas affected by electronic effluents, where the pH showed a complete lack of correlation ($r < 0.40$) with all ions due to highly heterogeneous local chemical disturbances.

Nitrogen compounds show a positive correlation between NO_3^- and NO_2^- ($r = 0.460$), as well as between NO_3^- and SO_4^{2-} ($r = 0.464$). Orthophosphates (PO_4^{3-}) are also strongly correlated with Ca^{2+} ($r = 0.655$) and Mg^{2+} ($r = 0.635$). The relationship between NO_3^- and SO_4^{2-} is consistent with studies carried out on the Oued-Souf Terminal Complex aquifer, where these two elements are associated with the same principal component (PC1), reflecting a common anthropogenic origin linked to agricultural fertilisation and the leaching of wastewater discharges. It is also consistent with the study by Barkat et al., which shows that agricultural activities and urban drainage networks promote the simultaneous infiltration of nutrients and soluble salts. The correlation between PO_4^{3-} and major cations is consistent with the study by Amina Hafsi et al. in the Skikda industrial zone, where the application of compound fertilisers promotes the joint leaching of phosphates and soil minerals.

TDS and electrical conductivity (EC) show very weak or negligible correlations with individual divalent ions, particularly between TDS and Ca^{2+} ($r = 0.037$). This result differs markedly from that of Egbueri et al., where TDS showed very strong linear correlations ($r > 0.89$) with all dissolved cations and anions. It also differs from the results from Ain Azel, where TDS and EC showed a correlation of $r = 0.96$ with the major salts. This difference suggests that, in the study catchment, total conductivity may result from complex polygenic contributions rather than from a single dominant salt.

Finally, OD shows significant positive correlations with Ca^{2+} ($r = 0.631$), Mg^{2+} ($r = 0.624$), PO_4^{3-} ($r = 0.635$) and SO_4^{2-} ($r = 0.580$). These relationships are consistent with the observations of Brindha et al., according to which the recharge of oxygenated meteoric water stimulates the chemical weathering of silicate and carbonate minerals and maintains the solubility of divalent ions. They are also consistent with the study by C. Jiang et al., which shows that the redox potential and the oxygenation state of the aquifer directly control mineral dissolution reactions.

Overall, the correlation matrix highlights the simultaneous influence of carbonate and evaporitic weathering processes, the physico-chemical conditions of the environment, and anthropogenic inputs in determining the composition of groundwater. The associations between nutrients and certain major ions particularly highlight the potential contribution of agricultural and

urban activities, whilst the weak correlations between TDS and EC with certain ions suggest that mineralisation is likely to be controlled by multiple factors.

4. CONCLUSION

This study provides a detailed hydrochemical characterisation of groundwater from wells and boreholes in three agricultural municipalities in the Hautes Plaines de Sétif: Mezloug, Guellal, and Bir Haddada. The results reveal that the groundwater is highly mineralised overall, with several parameters exceeding the WHO guideline values and the JORA regulatory limits. This is particularly evident in the high levels of electrical conductivity, total dissolved solids (TDS), total hardness, and concentrations of calcium, chlorides, and sulphates, as observed at stations S1 and S2. This high ionic load appears to be primarily linked to water–rock interactions, particularly the dissolution of carbonate and evaporite formations. This is compounded by changes in mineralisation from upstream to downstream, as well as the seasonal influence of soil leaching and rainfall recharge.

In terms of water quality, the S1 monitoring point is characterised by worrying levels of nitrate contamination, with maximum concentrations of 88.55 mg/L exceeding the WHO and JORA limits of 50 mg/L. This contamination is likely due to the diffuse leaching of nitrogen fertilisers used in surrounding agricultural areas, as well as inputs from domestic wastewater and on-site sewage treatment systems. In contrast, the nitrate concentrations recorded at stations S2 and S3 remain broadly in line with the relevant standards. The occasional exceedance of nitrite levels observed at S1 also highlights the need for targeted monitoring at this station.

Overall, the results highlight the high vulnerability of the studied groundwater bodies to natural and human-induced pressures in this semi-arid context. The combination of natural geochemical processes, seasonal soil leaching, agricultural activities, and domestic discharges contributes to the degradation of the groundwater resource's quality. To ensure the sustainable conservation of groundwater in the Sétif region, regular and continuous hydrochemical monitoring, the rationalisation of nitrogen fertiliser use, and protective measures around abstraction facilities appear to be management priorities.

ACKNOWLEDGEMENTS

I would like to express my deepest gratitude and sincere appreciation to Professor Bouharati Sedek and Professor Rouabhi Amar for their invaluable support, scientific expertise, and generous guidance, whose contributions have been instrumental in the successful completion of this article.

AUTHOR CONTRIBUTIONS

Benzidane Chahrazed*: Conceptualization, Writing, Data Curation, Investigation Formal Analysis.

Rouabhi Amar: Analysis, Formal Analysis.

Bouharati Sedek: Supervision, Writing—Review & Editing.

Fenni Mouhamed: Supervision, Writing—Review

CONFLICT OF INTEREST

The authors declare that there is no conflict of interest.

ETHICS STATEMENT

Ethical approval was not required for this study because it did not involve human participants, animals, or identifiable personal data.

DATA AVAILABILITY STATEMENT

The data supporting the findings of this study are available from the corresponding author reasonable request.

REFERENCES

[1] Abascal, E., Gómez-Coma, L., Ortiz, I. and Ortiz, A. (2022). Global diagnosis of nitrate pollution in groundwater and review of removal technologies. Science of the Total Environment, 810, 152233. https://doi.org/10.1016/j.scitotenv.2021.152233

[2] Dolor, C., Sit, D., 2023 Abdelbaki, H., Belkendil, A., Maazouzi, A. and Mekkaoui, A. (2022). Assessment of hydrochemical properties of groundwater in the alluvial aquifer of the arid zone of the Igli Region, South-West of Algeria. Desalination and Water Treatment, 268, 153–169. https://doi.org/10.5004/dwt.2022.28709

[3] Ali Rahmani, S.E. and Chibane, B. (2022). Geochemical assessment of groundwater in semiarid area, case study of the multilayer aquifer in Djelfa, Algeria. Applied Water Science, 12(3), 59. https://doi.org/10.1007/s13201-022-01573-y

[4] Aouiti, S., Hamzaoui-Azaza, F., Celico, F. and Zammouri, M. (2021). Groundwater quality assessment of Hajeb Layoun-Jelma aquifer (Central Tunisia) using hydrogeochemical and statistical approaches. Environmental Science and Pollution Research, 28(34), 46669–46691. https://doi.org/10.1007/s11356-020-11149-5

[5] Barkat, A., Bouaicha, F., Ziad, S., Mester, T., Sajtos, Z., Balla, D., Makhloufi, I., & Szabó, G. (2023). The integrated use of heavy-metal pollution indices and the assessment of metallic health risks in the phreatic groundwater aquifer—The case of the Oued Souf Valley in Algeria. Hydrology, 10(10), Article 201. https://doi.org/10.3390/hydrology10100201

[6] Bencheikh, A., Ziouch, O.R., Bensakhri, Z., Belksier, M.-S., Ben-Gusmia, D., Guastaldi, E., Bouznad, I.E. and Zebsa, R. (2025). Nitrate contamination in deep aquifers: Health risks and spatiotemporal analysis in an arid region of the Algerian Sahara. Desalination and Water Treatment, 322, 101239. https://doi.org/10.1016/j.dwt.2025.101239

[7] Benhedid, H., Achour, M., & Daddi Bouhoun, M. (2024). Exploring the spatial distribution of dissolved heavy metals and health risk assessment of cadmium in groundwater: A case study in Oued M'Zab region, Algeria. Environmental Health Engineering and Management, 11(1), 61–70. https://doi.org/10.34172/EHEM.2024.08

[8] Benmoussa, Y., Benkadi, Y. and Habi, M. (2020). Physico-chemical characterization and quality assessment of groundwater in Kerzaz and Beni Abbes oases (Saoura Valley, SW Algeria). Applied Water Science, 10(5), 125. https://doi.org/10.1007/s13201-020-01256-6

[9] Bioud, I., Semar, A., Laribi, A., Douaibia, S. and Chabaca, M.N. (2023). Assessment of groundwater quality and its suitability for irrigation: The case of Souf Valley phreatic aquifer. Algerian Journal of Environmental Science and Technology, 9(4), 1429–1435.

[10] Brindha, K., Paul, R., Walter, J., Tan, M. L., & Singh, M. K. (2020). Trace metals contamination in groundwater and implications on human health: Comprehensive assessment using hydrogeochemical and geostatistical methods. Environmental Geochemistry and Health, 42(11), 3819–3839. https://doi.org/10.1007/s10653-020-00637-9

[11] Bounab, S., Khemmoudj, K. and Sedrati, N. (2022). Assessment and physicochemical characterization of groundwater quality for irrigation and drinking purposes in Bazer Sakhra (Eastern Area of Algeria). Journal of Ecological Engineering, 23(8), 119–132. https://doi.org/10.12911/22998993/150696

[12] Brella, D., Belkhiri, L., Tiri, A., Salhi, H., Lakouas, F.E., Nouibet, R., Amrane, A., Merdoud, R. and Mouni, L. (2023). Identification of the groundwater quality and potential noncarcinogenic health risk assessment of nitrate in the groundwater of El Milia Plain, Kebir Rhumel Basin, Algeria. Hydrology, 10(8), 171. https://doi.org/10.3390/hydrology10080171

[13] Derdour, A., Jodar-Abellan, A., Ghoneim, S.S.M., Almaliki, A., Hussein, E.E. and Pardo, M.Á. (2023). Groundwater quality assessment for sustainable human consumption in arid areas based on GIS and water quality index in the watershed of Ain Sefra (SW of Algeria). Environmental Earth Sciences, 82(21), 510. https://doi.org/10.1007/s12665-023-11183-9

[14] Egbueri, J. C., & Unigwe, C. O. (2020). Understanding the extent of heavy metal pollution in drinking water supplies from Umunya, Nigeria: An indexical and statistical assessment. Analytical Letters, 53(13), 2122–2144. https://doi.org/10.1080/00032719.2020.1731521

[15] Eid, M. H., Tamma, A. A., Saeed, O., Székács, A., Abukhadra, M. R., El-Sherbeeny, A. M., Bence, C., Mikita, V., Kovács, A., & Szűcs, P. (2024). Advanced approach combines integrated weight water quality index and potential toxic elements for environmental and health risk assessment supported by simulation technique in Oued Souf, Algeria. Scientific Reports, 14(1), Article 17805. https://doi.org/10.1038/s41598-024-68854-1

[16] Hafsi, A., Bourefis, A., Kessasra, F., & Boushaba, A. (2024). Environmental assessment of pollution in an industrial environment using heavy metal pollution indices and stable isotopes, case study of the industrial zone of Skikda, North-East Algeria. Carpathian Journal of Earth and Environmental Sciences, 19(1), 33–50. https://doi.org/10.26471/cjees/2024/019/278

[17] Hakimi, Y., Orban, P., Deschamps, P. and Brouyere, S. (2021). Hydrochemical and isotopic characteristics of groundwater in the Continental Intercalaire aquifer system: Insights from Mzab Ridge and surrounding regions, North of the Algerian Sahara. Journal of Hydrology: Regional Studies, 34, 100791. https://doi.org/10.1016/j.ejrh.2021.100791

[18] Hao, W., Liu, H., Hao, S., & Mao, K. (2024). Characterization of heavy metal contamination in groundwater of typical mining area in Hunan Province. Scientific Reports, 14(1), Article 13054. https://doi.org/10.1038/s41598-024-63460-7

[19] Hamma, B., Alodah, A., Bouaicha, F., Bekkouche, M.F., Barkat, A. and Hussein, E.E. (2024). Hydrochemical assessment of groundwater using multivariate statistical methods and water quality indices (WQIs). Applied Water Science, 14(2), 33. https://doi.org/10.1007/s13201-023-02084-0

[20] Ismail, E., Alexakis, D.E., Abou Heleika, M., Hashem, M., Ahmed, M.S., Hamdy, D. and Ali, A. (2023). Applying geophysical and hydrogeochemical methods to evaluate groundwater potential and quality in Middle Egypt. Hydrology, 10(8), 173. https://doi.org/10.3390/hydrology10080173

[21] Jiang, C., Zhao, Q., Zheng, L., Chen, X., Li, C., & Ren, M. (2021). Distribution, source and health risk assessment based on the Monte Carlo method of heavy metals in shallow groundwater in an area affected by mining activities, China. Ecotoxicology and Environmental Safety, 224, Article 112679. https://doi.org/10.1016/j.ecoenv.2021.112679

[22] Kada, H., Demdoum, A., Baali, F., Aouati, H., & Djemel Eddine, H. (2022). Heavy metal contamination and exposure risk assessment via drinking groundwater in Ain Azel territory, north-eastern Algeria. Sustainable Water Resources Management, 8(5), Article 163. https://doi.org/10.1007/s40899-022-00748-4

[23] Manawi, Y., Subeh, M., Al-Marri, J., & Al-Sulaiti, H. (2024). Spatial variations and health risk assessment of heavy metal levels in groundwater of Qatar. Scientific Reports, 14(1), Article 15904. https://doi.org/10.1038/s41598-024-64201-6

[24] Mansouri, Z., Leghrieb, Y., Kouadri, S., Al-Ansari, N., Najm, H.M., Mashaan, N.S., Eldirderi, M.M.A. and Khedher, K.M. (2022). Hydro-geochemistry and groundwater quality assessment of Ouargla Basin, South of Algeria. Water, 14(15), 2441. https://doi.org/10.3390/w14152441

[25] Mebarki, S., Kharroubi, B. and Kendouci, M.A. (2021). Physicochemical evolution and evaluation of groundwater quality in Mougheul area (Southwest of Algeria). Applied Water Science, 11(2), 40. https://doi.org/10.1007/s13201-021-01368-7

[26] Mebarki, S., Tahri, M. and Mekkaoui, A. (2021). Hydrogeochemical characterization and quality assessment of the Jurassic aquifer in the Mougheul area (Bechar, SW Algeria). Applied Water Science, 11(4), 68. https://doi.org/10.1007/s13201-021-01368-7

[27] Medjani, F., Djidel, M., Labar, S., Bouchagoura, L. and Rezzag Bara, C. (2021). Groundwater physico-chemical properties and water quality changes in shallow aquifers in arid saline wetlands, Ouargla, Algeria. Applied Water Science, 11(5), 82. https://doi.org/10.1007/s13201-021-01415-3

[28] Mohammed, A.M., El-Sayed, M.I. and Mahmoud, A.A. (2022). Hydrogeochemical appraisal of groundwater quality for drinking and irrigation purposes in the Nile Aquifer System, Qena Governorate, Egypt. Applied Water Science, 12(7), 161. https://doi.org/10.1007/s13201-022-01611-9

[29] Mora, A., Torres-Martínez, J.A., Capparelli, M.V., Zabala, A. and Mahlknecht, J. (2022). Effects of wastewater irrigation on groundwater quality: An overview. Current Opinion in Environmental Science & Health, 25, 100322. https://doi.org/10.1016/j.coesh.2021.100322

[30] Nadjai, S., Bouderbala, A., Khammar, H., Nabed, A.N. and Benaabidate, L. (2024). Assessment of groundwater suitability for drinking and irrigation purposes in the middle Cheliff Aquifer, Algeria. Desalination and Water Treatment, 319, 100528. https://doi.org/10.1016/j.dwt.2024.100528

[31] Rawat, M., Sen, R., Onyekwelu, I., Wiederstein, T. and Sharda, V. (2022). Modeling of groundwater nitrate contamination due to agricultural activities—A systematic review. Water, 14(24), 4008. https://doi.org/10.3390/w14244008

[32] Selmane, T., Dougha, M., Djerbouai, S., Djemiat, D. and Lemouari, N. (2023b). Groundwater-quality evaluation based on water quality indices (WQI) using GIS: Maadher plain. Environmental Science and Pollution Research, 30(11), 30087–30106. https://doi.org/10.1007/s11356-023-25100-3

[33] Selmane, T., Dougha, M., Hasbaia, M., Ferhati, A. and Redjem, A. (2022a). Hydrogeochemical processes and multivariate analysis for groundwater quality in the arid Maadher region of Hodna, northern Algeria. Acta Geochimica, 41(5), 893–909. https://doi.org/10.1007/s11631-022-00553-y

[34] Ullah, Z., Rashid, A., Ghani, J., Nawab, J., Zeng, X.-C., Shah, M., Alrefaei, A. F., Kamel, M., Aleya, L., Abdel-Daim, M. M., & Iqbal, J. (2022). Groundwater contamination through potentially harmful metals and its implications in groundwater management. Frontiers in Environmental Science, 10, Article 1021596. https://doi.org/10.3389/fenvs.2022.1021596

[35] Wang, G., Guo, H., Zhang, J., Wang, J., Zhang, X., Li, B. and Wu, C. (2024). Source apportionment and hydrogeochemical controls of nitrate contamination in shallow groundwater of Sha River Basin. Scientific Reports, 14, 16773. https://doi.org/10.1038/s41598-024-67735-x .

[36] Wang, L., Tao, Y., Su, B., Wang, L., & Liu, P. (2022). Environmental and health risks posed by heavy metal contamination of groundwater in the Sunan Coal Mine, China. Toxics, 10(7), Article 390. https://doi.org/10.3390/toxics10070390